EUROfusion

EUROFUSION CP(15)04/09

A. Weckmann et al.

Local Migration Studies of High-Z Metals in the TEXTOR Tokamak

(18th May 2015 – 22nd May 2015)
Aix-en-Provence, France

This work has been carried out within the framework of the EUROfusion Consortium and has received funding from the Euratom research and training programme 2014-2018 under grant agreement No 633053. The views and opinions expressed herein do not necessarily reflect those of the European Commission.

Local migration studies of high-Z metals in the TEXTOR tokamak

A. Weckmann[1], P. Petersson[1], M. Rubel[1], P. Wienhold[2], S. Brezinsek[2], J. W. Coenen[2], A. Kirschner[2], A. Kreter[2], A. Pospieszczyk[2]

[1]*Fusion Plasma Physics, Royal Institute of Technology (KTH), 100 44 Stockholm, Sweden*
[2]*Institute for Energy and Climate Research (IEK-4, Plasma Physics), Forschungszentrum Jülich, 52425 Jülich, Germany*

Abstract

Volatile compounds of tungsten (WF_6) and molybdenum (MoF_6) were used as tracers of high-Z metal migration in the TEXTOR tokamak in several gas injection experiments when puffing was done through a test limiter. The experiments with W were performed prior major shut-downs, while the MoF_6 was followed by the final shutdown in connection with TEXTOR decommissioning. In all cases a set of various surface probes and limiter tiles were retrieved and analysed with electron and ion beam techniques. The focus was on the local deposition in the vicinity of the gas inlet and in the inlet system. Depth profiles in the deposits and metal distribution maps clearly shown that only near the gas inlet significant amounts of Mo are deposited along the scrape-off layer flow and E×B drift directions, which could be reproduced by ERO-code modelling. Correlation between the plasma operation scenario and the deposition patterns is presented.

Keywords: *Tracer materials, Molybdenum, Tungsten, Nitrogen, Erosion-Deposition, TEXTOR*

**Corresponding author E-mail: weckmann@kth.se*

Introduction

Studies of high-Z metals such as tungsten and molybdenum for plasma-facing components (PFCs) in magnetic controlled fusion devices have a long history, as summarised in [1-3]. The recent decision to use a full tungsten divertor from day 1 in the International Thermonuclear Experimental Reactor (ITER) has been preceded by comprehensive studies and investments including the installation of the ITER-Like Wall (ILW) in the JET tokamak: beryllium in the main chamber and tungsten in the divertor [4]. The elimination of carbon from the high-heat flux (HHF) zone of a reactor wall has been dictated by the need for a significant reduction of fuel inventory [1, 5-9]. Material challenges, though of other nature, still remain as the W-based HHF components will suffer from erosion and melting [9]. Both effects lead to the release of tungsten and result in damaged PFC surfaces, likely to affect plasma performance due to massive radiative cooling [10] while the damage of PFCs limits their lifetime and can enhance erosion even more [9]. A mechanism of prompt re-deposition may diminish both negative effects: eroded particles may directly return to their place of origin, or close to it, as they get ionised and gyrate in the magnetic field back to the surface [11]. However, prompt re-deposition does not prevent fairly effective long-range W migration [12].

A set of experiments was conducted in the TEXTOR tokamak [13] in order to tackle two issues: (i) the local versus global transport of high-Z metals, (ii) the deposition and retention in wall materials of nitrogen used for edge cooling in operation with heavy metals [14,15]. For this tungsten hexafluoride (WF_6) and nitrogen-15 marker gas ($^{15}N_2$) were injected before major shut-downs in 2008 and 2011 [12]. In the last experiment at TEXTOR, before the machine decommissioning, MoF_6 and $^{15}N_2$ were injected (late 2013).

Due to the importance of material migration (erosion, transport and deposition) in general, much effort is put into developing simulation codes in order to model material migration. For

local migration, ERO-code has been successfully benchmarked against gas injection experiments at TEXTOR [17,18].

This paper addresses the local deposition patterns of Mo found on top of the test limiter at and inside the gas injection channels as well as the comparison between experimental Mo deposition patterns and simulated patterns from the ERO code. It furthermore addresses the deposition of Mo and W in the inlet system, an issue important for experiments based on hexafluoride gases for Mo or W seeding in impurity transport experiments [12,16] but also in-vessel coating of PFCs with W [19,20]. The focus is on the following points: (i) local deposition efficiency of Mo; (ii) ERO modelling of the experimental data to identify processes governing the deposition; (iii) comparison of high-Z seeding gasses, MoF_6 and WF_6, as the transport markers; (iv) clarification of high-Z metals deposition in the injection system.

Experimental

2.1. Experimental conditions in TEXTOR

The experiments were carried out in the TEXTOR tokamak, Forschungszentrum Jülich, Germany, which was in operation until December 2013. It was a medium-size limiter machine with a circular cross-section: R=1.75 m, a=0.47 m, plasma volume of about 7 m^3 [21]. Its main scientific mission was focused on the understanding and control of plasma-wall interactions (PWI) processes including material testing, development of diagnostic tools and methods and procedures for studies and description of material migration. The latter included the development of tracer techniques, from carbon to high-Z metals, based on a controlled injection of marker gases or exposure of probes and instrumented (marker) tiles [22-26].

In the last experiment at TEXTOR volatile Mo compound was used because earlier experiments with WF_6 injection and test limiters [12,16] left a significant W background. MoF_6 was chosen although there were some experiments with Mo in the past and this element is a constituent of the Inconel 625 liner [27], which contains around 4.7 at% Mo (9 wt%) [28].

Puffing of MoF_6, as in the case of experiments with WF_6, was realised through a special roof limiter inserted at the bottom of the vessel (Fig. 1 a, arrow indicating plasma current direction) with its tip at r=47,5 cm, i.e. 0,5 cm behind the last closed flux surface (LCFS). The test limiter assembly, shown schematically in Fig. 2, consisted of a top plate (collector plate) made of 2 mm thick polished graphite with a hole for gas injection (1), a roof-shaped graphite block with an injection channel (2), sealing (3) and a metal base plate (4).

The discharges lasted 8 s with MoF_6 injection from 0.8 s to 1.8 s through the Limiter Lock 1 (LL1, detail of the lock in [29]) at the bottom of the vacuum vessel, ^{15}N injection from 1 s to 5 s through the fast gas feed in section 14/15 and neutral beam co-injection heating by NBI-1 with power of 1.7 MW from 0.8 s to 5.3 s. A schematic timeline is displayed in Fig. 1(b). The toroidal field strength was 2.25 T, the plasma current was 350 kA and directed in counter-clockwise direction, as seen from above (standard TEXTOR configuration). During the experiment two disruptions occurred because of density increase caused by high outgassing of nitrogen from the walls. To enable tokamak operation He glow wall conditioning was applied for 5 minutes every 3-5 tokamak pulses with a wall potential of approximately 300 V.

For determination of the total deposition efficiency it was important to quantify the amount of MoF_6 which was injected during 31 discharges. The amount released from the calibrated volume in the inlet system could be determined as for other gasses by pressure drop in the volume, which was thus estimated to be around $1.42 \cdot 10^{21}$ molecules. However, spectroscopic evaluation of the MoI line (388 nm) intensity directly at the gas inlet yield about 40% of the

molecules leaving the calibrated volume, or around $5.7 \cdot 10^{20}$ molecules.

2.2. Analysis methods

Local spectroscopic measurements during the high-Z gas injection experiments were performed using systems described in [30]. Cameras and imaging spectrometer (Acton Research Corporation, model SpectraPro 500) with a holographic grating in Czerny-Turner arrangement were used at a central wavelength of 395 nm to cover both FII (402 nm) and MoI (388 nm) lines visible during the injection. The fluxes at the SOL were estimated from the S/XB line ratio: nitrogen accounted for 5-10 % of the total flux.

Calibration of line emission to the injected gas amount was conducted successfully for WF_6 [16]. In order to estimate the MoF_6 amount following adaptions were necessary: (i) a calibration factor of the camera (photons/counts) similar to that for the WI line was assumed; (ii) a transmission coefficient of the MoI filter similar to the WI filter was assumed; (iii) a photon yield from excited atoms or molecules (S/XB value) of 1 similar to the MoI line at 379 nm was used.

MoF_6 has its boiling point at 34°C and a vapour pressure of 101.3 kPa at 33.5°C [31]. This results in an estimated vapour pressure of 50.56 kPa at room temperature, which is also the temperature of the calibrated volume of the gas inlet system of TEXTOR, estimated from an exponential fit of the temperature values given for 1, 10 and 100 kPa in [31]. This approximate value is in accordance with the values in [32]. MoF_6 is a very heavy gas: 209.93 u/mol [31]. As a consequence it reaches the torus with a 0.4 s delay between the valve opening and MoI line appearance, see Fig. 3. Such a delay was also seen for the WF_6 injection reported in [12]. Since it cannot be excluded that a considerable amount of MoF_6 released from the calibrated volume resided in the pipes between the calibrated volume and the vessel,

the spectroscopic estimation of $5.7 \cdot 10^{20}$ molecules will be used for reference of the deposition efficiency.

After all gas puffing experiments and the retrieval of tiles and probes ex-situ surface studies were performed for the plate on the test limiter. In addition, in the case of the MoF_6 injection detailed examination was extended to parts of the gas inlet module to assess the deposition in that system, respective parts are marked in Fig. 2. Surface composition of the top plate (1) was measured with electron probe micro analysis (EPMA) with 15 kV along several lines of analysis at RWTH Aachen, Germany. Due to the deposit thickness the measurements were repeated with a 30 kV beam along two lines close to the injection hole, but still the full layer thickness could not be probed. Hence, two points near the hole were analysed with secondary ion mass spectroscopy (SIMS) in order to estimate the layer thicknesses and provide data for extrapolation. The sample was bombarded with a Cs^+ beam of 141 nA and a crater of 300 µm×300 µm. Its depth was determined with a laser profilometer thus yielding a sputter rate with SIMS of 0.89 nm/s. Another point directly at the injection hole was additionally probed with time-of-flight heavy ion elastic recoil detection analysis (ToF-HIERDA) [33] for the quantification and cross-checking the upper layer in the SIMS depth profile. HIERDA with a 36 MeV $^{127}I^{8+}$ beam is suitable for quantitative depth profiling of low- to medium-Z elements of up to 600 nm in carbon-reach target with resolution of a few nm.

A coloured pattern developed on the graphite block (2) though it was shielded by the top collector plate against direct plasma exposure. This pattern was examined along the toroidal direction for high-Z elements with Rutherford backscattering (RBS) [34] using a 2 MeV $^4He^+$ beam. Then the graphite block was sawn up in order to determine by means of RBS the presence of Mo and W inside the injection channels. Finally, the stainless steel base plate (4) was examined with RBS right at the position of the sealing (3) between the plate and the graphite block because deposits were clearly visible. The sealing had been provided by an O-

ring, which could not be examined but a rectangular area (3×20 mm) around the ring was scanned in millimetre steps, thus providing data for area close and further away from the valve.

2.3. Modelling

The modelling of deposition on the plate was conducted with the ERO code for the area 1 cm away from the LCFS with following parameters: electron temperature T_e=30 eV, e-folding length $\lambda(T_e)$ of 40 mm, ion temperature T_i=60 eV, $\lambda(T_i)$ of 40 mm, averaged edge electron density $n_e=5\cdot10^{12}$ cm^{-3}, $\lambda(n_e)$ 30 mm; and impurity fluxes of C^{4+} (5,2%) and O^{5+} (1%). Since no dissociation data of MoF_6 are incorporated in the ERO code, Mo atom injection of around 0.1 eV Maxwell distributed energy and 0° injection angle (along radial direction) was taken for modelling in order to match spectroscopic data. Fig. 4 shows the comparison of the camera image at the limiter and the modelled distribution of MoI species.

3. Results and discussion

3.1. Local deposition: experiment and model

The top plate after the exposure is shown in Fig. 5(a). The shiny-looking deposit is not uniform. It stretches toroidally from the gas inlet to the upper right corner as a result of the SOL flow [25] and the E×B drift to the high field side [38]. This pattern agrees with earlier findings in marker experiments involving WF_6 and $^{13}CH_4$ [12,25]. However, after the MoF_6 injection the elongated deposition in the toroidal direction is less pronounced than that for $^{13}CH_4$ [25]. Maps of the tungsten deposition obtained with EPMA and by ERO modelling are in Fig. 5(b) and (c), respectively. One perceives that the Mo concentration distribution corresponds to the general deposition pattern. Also the modelled profile presents an area stretching toroidally towards the high field side, i.e. reflects the experimental findings. SIMS

yielded a deposition layer thickness of 1,6 μm at a point 4 mm away from the gas inlet and 6 μm at a point located less than mm from the inlet, i.e. in red circle and blue circles, respectively in Fig. 5(a). The depth of the craters in these two points is shown in Fig. 6(a), while plots in Fig. 6(b) represent the variation of carbon and molybdenum in the deposit formed next to the gas inlet. They are associated with the experimental conditions that included disruptions and also He glow for wall conditioning. Fine structure of the deposition in the top 400 nm obtained with ToF-HIERDA near the gas inlet is shown in Fig. 7 which reflects the history in the last phases in the experiment. There is a qualitative agreement between the SIMS and ERDA for C and Mo.

The overall amount of Mo on the collector plate is $3.5 \cdot 10^{19}$ atoms, which yields a deposition efficiency of about 6% of the puffed amount taking into account the actual injection of 5.7×10^{20} atoms. It should be stressed that this result is in agreement with the early data in [41], where the injection of a larger amount of Mo was taken into account: 3% of 1.42×10^{21}.

ERO simulation of Mo injection through the roof limiter yielded 81% local deposition efficiency instead of the experimentally obtained 6%. Therefore, the model needed to be adapted in order to yield the aforementioned 6% deposition efficiency: It was assumed that for each Mo atom being re-deposited on the collector plate six fluorine atoms also return to the surface (fluorine sputter yield on Mo: Y_F=1%), and that the physical sputtering of deposited Mo is enhanced by a factor of 15 due to its lower surface binding in comparison to bulk Mo. This is a method also applied in the simulation of other gas injection experiments and it is further discussed in [39]. Furthermore, as the deposited film contains mainly C the sputtering yield of Mo in a Mo-C mixture may actually be more close to pure carbon instead of pure Mo as it is the case for mixed C-W layers [40]. In summary, the quantitative

discrepancy in the deposition efficiency between the experiment and modelling points to the need for studies of deposition in the gas injection system.

3.2. Analysis of the gas injection system

Fig. 8(a) and (b) show, respectively, the appearance of the graphite block and Mo content distribution on that block below the top plate. Colour fringes are characteristic for deposits of less than 1 μm in thickness. Since the Mo concentration surmounts lighter elements other than carbon it is possible to evaluate the layer thickness from the RBS spectra: between several 100 nm peaking at 500 nm near the hole of the injection channel. This is in accordance with estimates done on the basis of the interference fringe order, assuming carbon as main element in the fringe, estimating the maximum thickness to be around 300 – 400 nm. In fact, the RBS results suggest besides a high Mo content (up to 1.8%) mainly O (3-10%), N (3-5%) and C+B (85-92%).

The same block was used in earlier injection experiments with WF_6. Indeed, tungsten is also traceable on the block though its deposition pattern does not coincide with the colour fringes. The areal concentration outside the colour fringes is within the same order of magnitude as for Mo. Very precise quantification of W is difficult in the presence of Mo majority, however, with a maximum measured areal concentration of around $6x10^{14}$ cm^{-2} an upper estimation of W can be given by assuming the highest concentration on the whole surface of 89.6 cm^2 the total amount is $5.2 \cdot 10^{16}$ atoms. This can be rated negligible to the amounts used in WF_6 tracer experiments: around $2x10^{20}$ [12]. This indicates that the residence of Mo from the MoF_6 decomposition in the pipes is significantly greater than that of W.

Data in Fig. 9 show results for analysis of the injection channels. There is an alternating deposition pattern along the small injection channel while the deposition in the more remote,

big channel decreases in the direction to the gas feeding tube to a constant level. The amount of Mo in the small channel is about $1x10^{17}$ atoms, while in the bigger channel it is about $1.6 \cdot 10^{17}$ atoms. The overall amount of Mo in the inlet channels of the roof limiter amounts to $2.6 \cdot 10^{17}$ atoms or 0.05% of the puffed amount.

As for the graphite block, the quantification of the W amount is more difficult than it is for Mo. Comparing the maximum peak heights in RBS of both elements, the total W would amount to 4% of the Mo amount in the small channel (i.e. $4x10^{15}$ atoms) and 10% of the Mo amount in the big channel (i.e. $1.6 \cdot 10^{16}$ atoms). This estimate, though rather rough, shows clearly the trend. Qualitatively, the W pattern coincides with the Mo signal both in the small and the bigger channel. In the search for W and Mo in the block even a very improbable possibility was checked: the diffusion of metals into the graphite block. It was sawn and the bulk was analysed: neither Mo nor W could be found.

The last analysed part was the steel base in the area of the sealing: RBS measurements of a 3×20 mm rectangle covered about 25% of the area near the sealing. The maximum areal concentration of Mo found is ca. $5x10^{14}$ cm^{-2}, with an average of ca. $1x10^{14}$ cm^{-2}. Most Mo was found around the sealing. The quantification problem former encountered just for W is also present here for Mo. An upper estimation of the Mo in the sealing area was done by assuming the maximum concentration found and multiplying it with the area size where the Mo was mainly found. The upper estimation yields ca. $9.5x10^{16}$ Mo atoms, which is less than 0.02% of the puffed amount.

The areal W concentration was far lower with a maximum of $7x10^{13}$ cm^{-2} and an average of $2x10^{13}$ cm^{-2}. It was also less concentrated around the sealing area but instead higher in the periphery of the probed area. An upper estimation was therefore calculated by assuming the maximum concentration found multiplied with the area of the base plate, yielding an upper

estimation of ca. $4.2 \cdot 10^{15}$ W atoms. In both cases the amounts of Mo and W found on the base plate are negligible to in comparison to injected amounts in gas puffing experiments.

The overall amounts found on different parts of the inlet system are given in Table 2. These data are given after careful analysis of the sources of errors and uncertainties connected with respective analysis techniques. EPMA results suffer from uncertainties related to the surface roughness and are estimated to be not higher than 16% for Mo, with quantitative errors around 5% [35] and errors due to surface roughness of maximum 15% [36], assuming a surface roughness of 0.1μm for the polished graphite [37]. SIMS uncertainties in depth result mainly from irregular sputtering and are about 0.2-0.5μm, depending on sputtering depth. RBS uncertainties are 15-20% for both Mo and W values due to some uncertainties in stopping cross-section [34], current integration and statistical error. In summary, the data inform that the Mo amount found on the top plate (3.5×10^{19}) is nearly 50 times larger than the amount in the gas injection system. The amount of tungsten from earlier experiments in the channels is small in comparison to the amount of Mo.

4. Concluding remarks

An important contribution of this work to the high-Z migration studies is related to the combination of a very comprehensive analysis and modelling of phenomena at the local source. The experiment at TEXTOR gave a great opportunity to determine both the gas injection (spectroscopy) and detailed ex-situ analyses of the test limiter. The local deposition of Mo governed by the SOL flow and the E×B drift could be qualitatively reproduced by the ERO modelling. However, a very high re-erosion factor (15) is to be implemented in modelling in order to match the experimentally determined deposition efficiency which is around 6%. It may indicates that Mo is re-eroded as efficiently as carbon species with which molybdenum is co-deposited on the plate near the gas inlet. It can be considered as a starting

point for the efficient long-range transport of high-Z in the torus. The importance of re-erosion – prompt re-deposition cycle was shown in [12]. The study on the global pattern in the Mo transport is continued. Over 200 wall tiles were retrieved for the ex-situ examination in order to map the metal distribution in deposits in the torus. Also dust samples collected from a large number of locations have been studied. The presence of Mo has been identified though its origin is associated not only with the experiment described above [42].

Acknowledgments

This work has been carried out within the framework of the EUROfusion Consortium and has received funding from the European Union's Horizon 2020 research and innovation programme under grant agreement number 633053. The views and opinions expressed herein do not necessarily reflect those of the European Commission. The work has been partly funded by the Swedish Research Council (VR) through contract no. 621-2009-4138.

References

[1] Tanabe T Noda N and Nakamura H 1992 *J. Nucl. Mater.* **196-198** 11
[2] Federici G *et al* 2001 *Nucl. Fusion* **41** 1967
[3] Philipps V 2013 *J. Nucl. Mater.* **415** S2
[4] Matthews GF et al 2011 *Phys. Scr.* **T145** 014001
[5] Coad JP et al 2001 *J. Nucl. Mater.* **290-293** 224
[6] Rubel M et al 2003 *J. Nucl. Mater.* **313-316** 321
[7] Loarer T et al 2007 *Nucl. Fusion* **47** 1112
[8] Brezinsek S *et al* 2013 *Nucl. Fusion* **53** 083023
[9] Pitts R A *et al* 2013 *J. Nucl. Mater.* **438** 48-56
[10] McCracken G M and Stott P E 1979 *Nucl. Fusion* **19** 889-981
[11] Naujoks D *et al* 1996 *Nucl. Fusion* **36** 671-87
[12] Rubel M *et al* 2013 *J. Nucl. Mater.* **438** 170-174
[13] Neubauer O *et al* 2005 *Fusion Sci. Technol.* **47** 76-86
[14] Kallenbach A et al 2011 *J. Nucl. Mater.* **415** S19

[15] Brezinsek S et al 2011 *Nucl. Fusion* **51** 073007

[16] Brezinsek S *et al* 2011 *Phys. Scr.* **T145** 014016

[17] Kirschner A *et al* 2000 *Nucl. Fusion* **40** 989-1001

[18] Droste S *et al* 2008 *Plasma Phys. Contr. Fusion* **50** 015006

[19] Philipps V *et al* 2011 *Phys. Scr.* **T145** 014030

[20] Cambe A *et al* 2001 *Fusion Eng. Des.* **56-57** 331-6

[21] Samm U 2010 *Fusion Sci. Technology* **57** 241-6

[22] Wienhold P *et al* 2003 *J. Nucl. Mater.* **313-316** 311-320

[23] Wienhold P *et al* 2001 *J. Nucl. Mater.* **290-293** 362-366

[24] Kirschner A *et al* 2005 *Fusion Sci. Technol.* **47** 146-160

[25] Kreter A *et al* 2007 *J. Nucl. Mater.* **363** 179-83

[26] Petersson P et al 2012 *Nucl. Instrum. Meth.* **B273** 113

[27] Brandt B *et al* 1986 *Fusion Technol.* **1** 601-6

[28] Special Metals Corporation, 2013. http://www.specialmetals.com/documents/Inconel%20alloy%20625.pdf

[29] Schweer B *et al* 2005 *Fusion Sci. Technology* **47** 138-45

[30] Brezinsek S *et al* 2005 *Plasma Phys. Contr. F.* **47** 615-34

[31] Handbook of Chemistry and Physics, CRC, 2014. http://www.hbcpnetbase.com/

[32] Ruff O and Ascher E 1931 *Z. Anorg. Allg. Chem.* **196** 413-20

[33] Whitlow H J, Possnert G and Petersson C S 1987 *Nucl. Instrum. Methods* **B27** 448-57

[34] Baumann S M 1992 *Encyclopedia of Materials Characterization* ed Brundle C R *et al* (Stoneham: Butterworth-Heinemann) 476-87

[35] Newbury D E 1992 *Encyclopedia of Materials Characterization* ed Brundle C R *et al* (Stoneham: Butterworth-Heinemann) 175-91

[36] Yamada A *et al* 2003 *Thin Solid Films* **431-432** 277-83

[37] Kreter A *et al* 2008 *Plasma Phys. Contr. Fusion* **50** 095008

[38] Lehnen M *et al* 2003 *Nucl. Fusion* **43** 168-78

[39] Kirschner A *et al* 2011 *J. Nucl. Mater.* **415** 239-45

[40] Taniguchi M *et al* 2003 *J. Nucl. Mater.* **313-316** 360-3

[41] Rubel M *et al* 2015 *J. Nucl. Mater.* in press.

[42] Fortune E *et al* 2015 *This conference*

Table 1: Overall quantitative results for Mo and W on different parts of the test limiter.

Location	**Average /Maximum Mo content (cm^{-2})**	**Total Mo amount (at)**	**Average /Maximum W content (cm^{-2})**	**Total W amount (at)**
Collector plate	$3{,}9\cdot10^{17}$ / $1{,}2\cdot10^{19}$ §	$3{,}5\cdot10^{19}$	Not identified	--
Graphite block surface	$2{,}1\cdot10^{16}$ * / $3{,}8\cdot10^{16}$	$4{,}4\cdot10^{17}$	$1{,}2\cdot10^{14}$ # /$6.0\cdot10^{14}$	$\leq5{,}2\cdot10^{16}$
Graphite block channels	$3{,}6\cdot10^{16}$ / $8{,}1\cdot10^{16}$	$2{,}6\cdot10^{17}$	$8{,}5\cdot10^{14}$ /$1{,}4\cdot10^{15}$	$\sim2\cdot10^{16}$
Base plate	$1{,}5\cdot10^{16}$ /$6{,}8\cdot10^{16}$	$\leq9{,}5\cdot10^{16}$	$3{,}1\cdot10^{15}$ / $8{,}9\cdot10^{15}$	$\leq4{,}2\cdot10^{15}$
Total	-	**$\leq3{,}58\cdot10^{19}$**	-	**$\leq7{,}6\cdot10^{16}$**

*§ extrapolation from EPMA data, *in the colour fringes, # on the whole surface*

Figure captions

Fig. 1: a) Graphite limiter with collector plate on top. The arrow indicates toroidal direction along the plasma current; **b)** Timeline of the experiment with the MoF_6 and $^{15}N_2$ injection.

Fig. 2: Schematic drawing of the gas inlet system part, which was examined for this paper: (1) Collector plate; (2) graphite block; (3) O-ring; (4) stainless steel base plate. The inclination of the limiter is 20°. The red arrow indicates the gas flow through the system.

Fig. 3: Local spectroscopic measurement at the gas inlet. “start” and “end” delimit the MoF_6 gas puffing phase.

Fig. 4: MoF_6 injection: (a) camera image recorded from the horizontal observation port at TEXTOR and (b) ERO simulation of MoI light.

Fig. 5: Deposition on the top collector plate: (a) appearance of the plate with marked areas or analysis (EPMA 15 kV, white thin arrows; 30 kV, yellow thick arrows – only a few lines shown for the image clarity, SIMS red and blue circles and ToF HIERDA slightly above the blue; (b) Mo distribution based on EPMA and (c) ERO simulation.

Fig. 6: Depth profiling of deposits: (a) stylus profilometer crater profiles in two points studied by SIMS; (b) distribution of carbon and molybdenum on the top plate near the gas inlet.

Fig. 7: Top layer measurement of the first 400 nm with ToF-HIERDA.

Fig. 8: (a) Colour fringes on the graphite block right underneath the top collector plate with points of measurement for RBS; (b) RBS results for Mo analysis.

Fig. 9: RBS measurements inside the channels of the graphite block, signals from Mo (blue diamonds) and W (multiplied by 20, red squares). The encircled measurement point was performed on substrate. Injection gas flow is indicated by white arrows.

a)

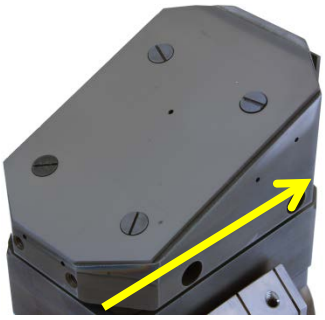

b)

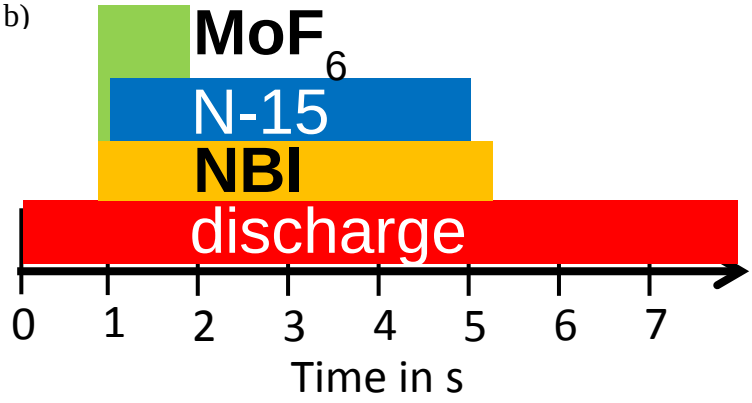

Fig. 1: (a) Graphite limiter with the top collector plate on top. The arrow indicates toroidal direction along the plasma current; (b) Timeline of the experiment with the MoF_6 and $^{15}N_2$ injection.

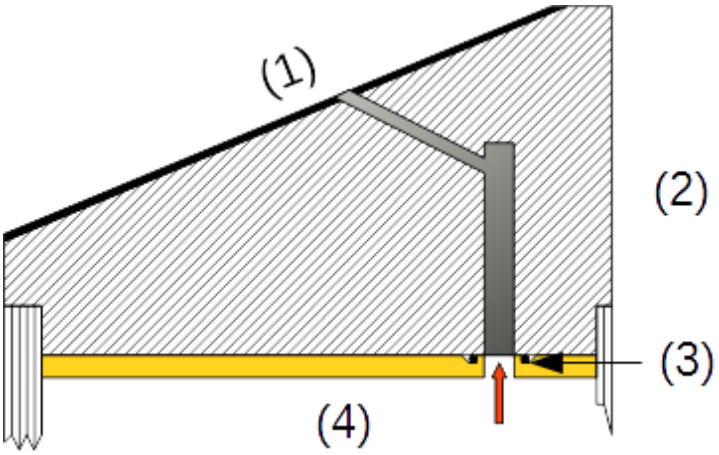

Fig. 2: Schematic drawing of the gas inlet system part, which was examined for this paper: (1) Collector plate; (2) graphite block; (3) O-ring; (4) stainless steel base plate. The inclination of the limiter is 20°. The red arrow indicates the gas flow through the system.

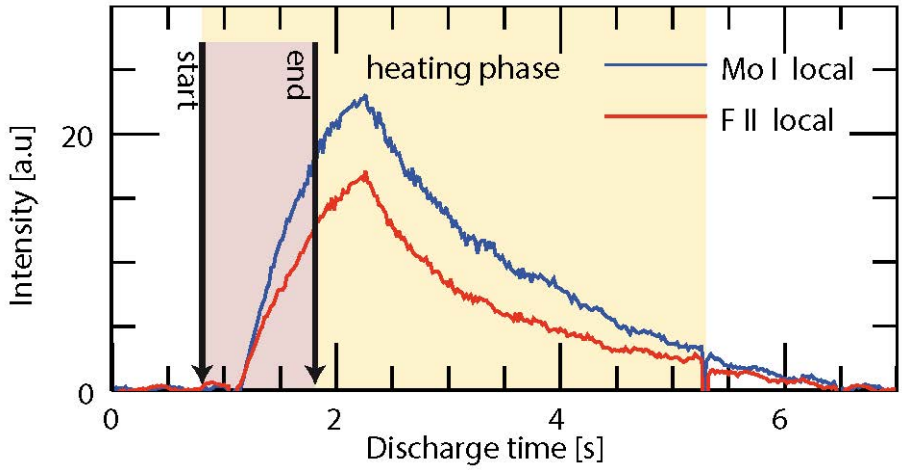

Fig. 3: Local spectroscopic measurement at the gas inlet. “start” and “end” delimit the MoF_6 gas puffing phase.

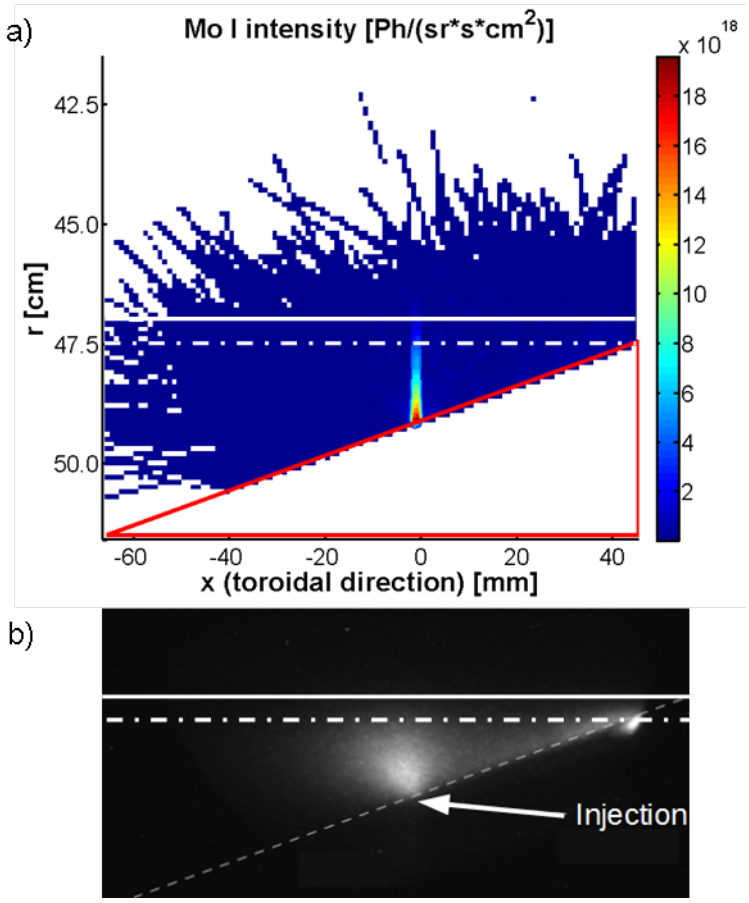

Fig. 4: MoF_6 injection: (a) ERO simulation of MoI light and (b) MoI camera image recorded from the horizontal observation port at TEXTOR with roof tip at 47.5cm of the plasma radius (dash-dotted line) and the LCFS at 47cm (solid line).

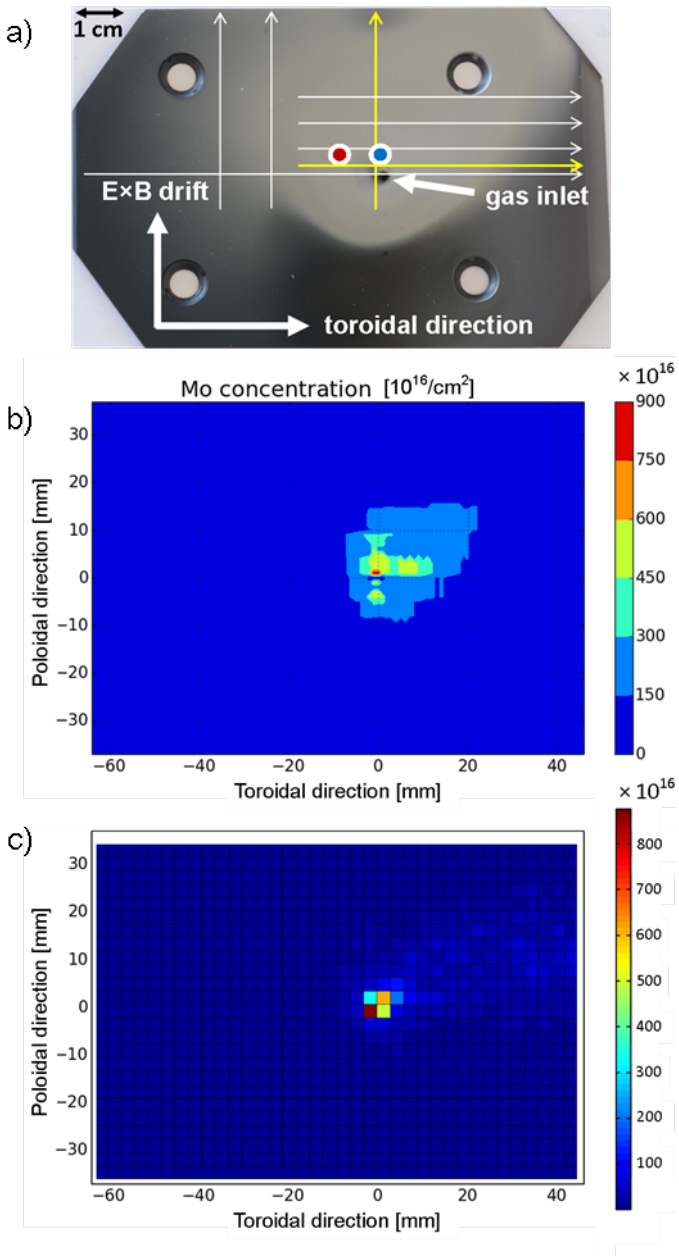

Fig. 5: Deposition on the top collector plate: (a) appearance of the plate with marked areas or analysis (EPMA 15 kV, white thin arrows; 30 kV, yellow thick arrows – only a few lines shown for the image clarity, SIMS red and blue circles, ToF ERDA slightly above the blue circle; (b) Mo distribution based on EPMA and (c) ERO simulation.

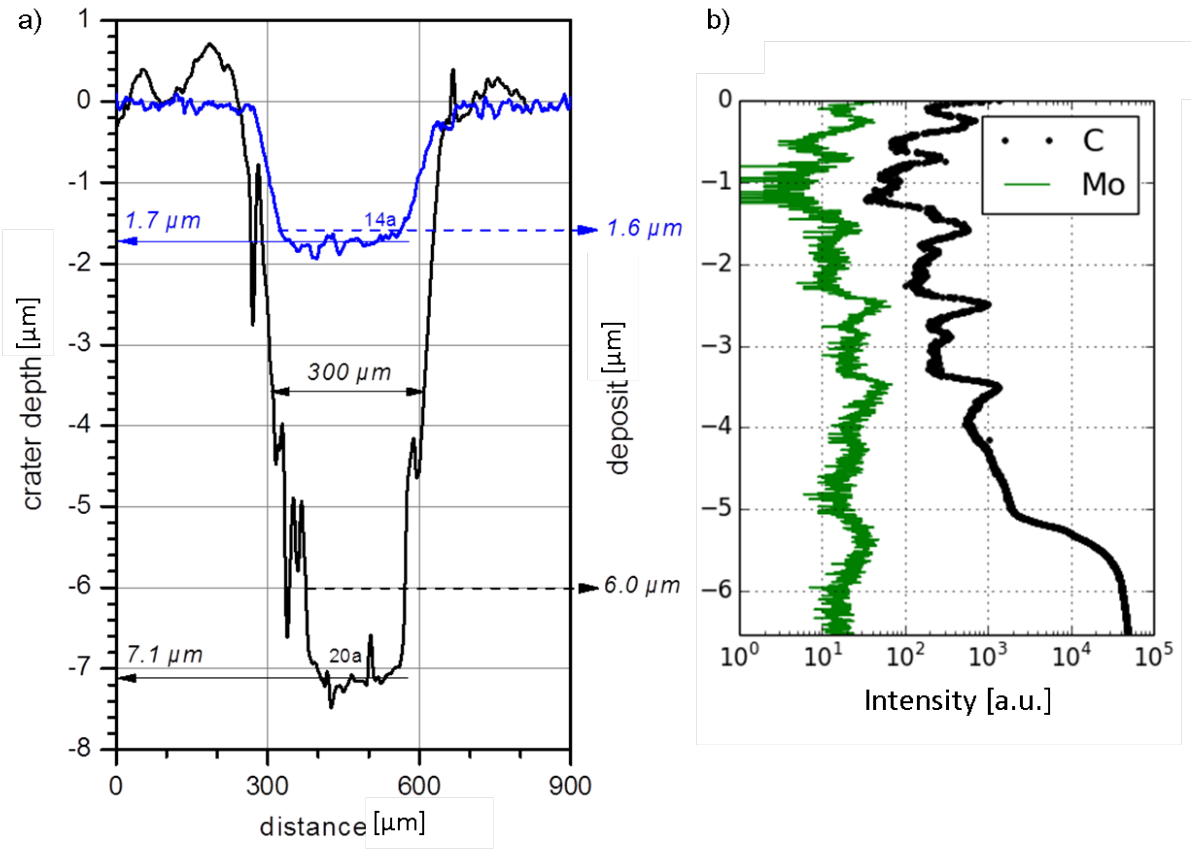

Fig. 6: Depth profiling of deposits: (a) stylus profilometer crater profiles in two points studied by SIMS; (b) distribution of carbon and molybdenum on the top plate near the gas inlet measured with SIMS.

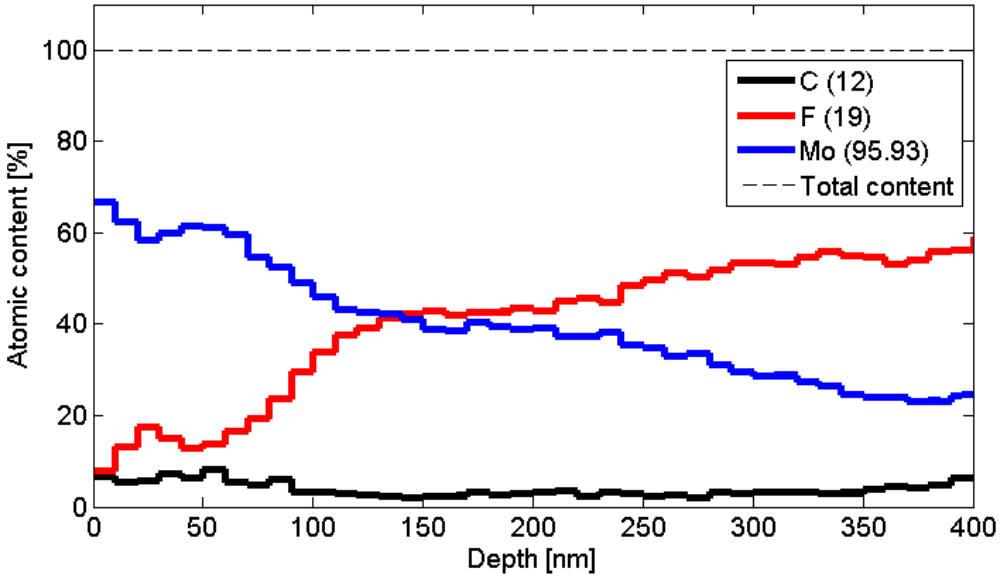

Fig. 7: Top layer measurement of the first 400 nm with ToF-HIERDA.

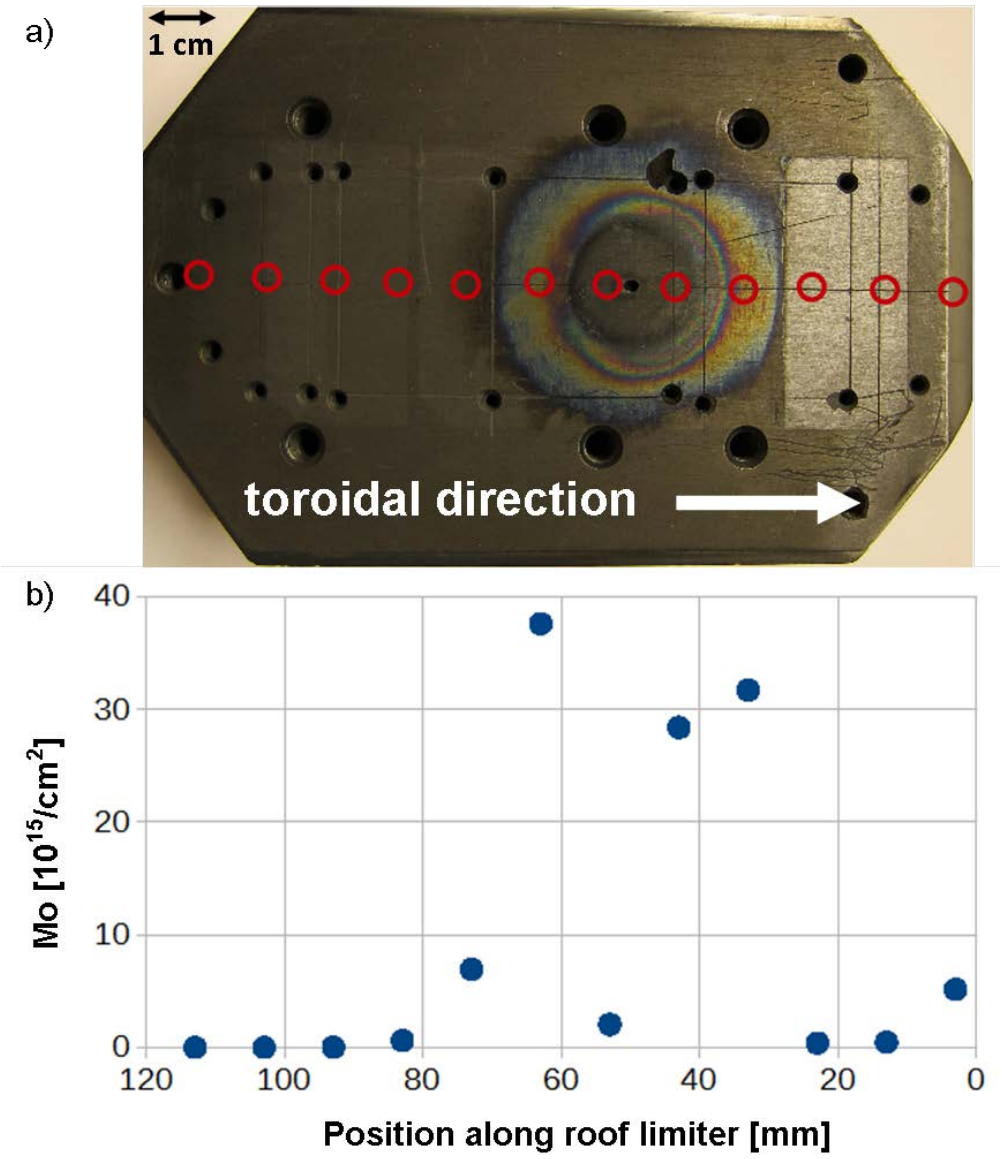

Fig. 8: (a) Colour fringes on the graphite block right underneath the top collector plate with points of measurement for RBS; (b) RBS results for Mo analysis.

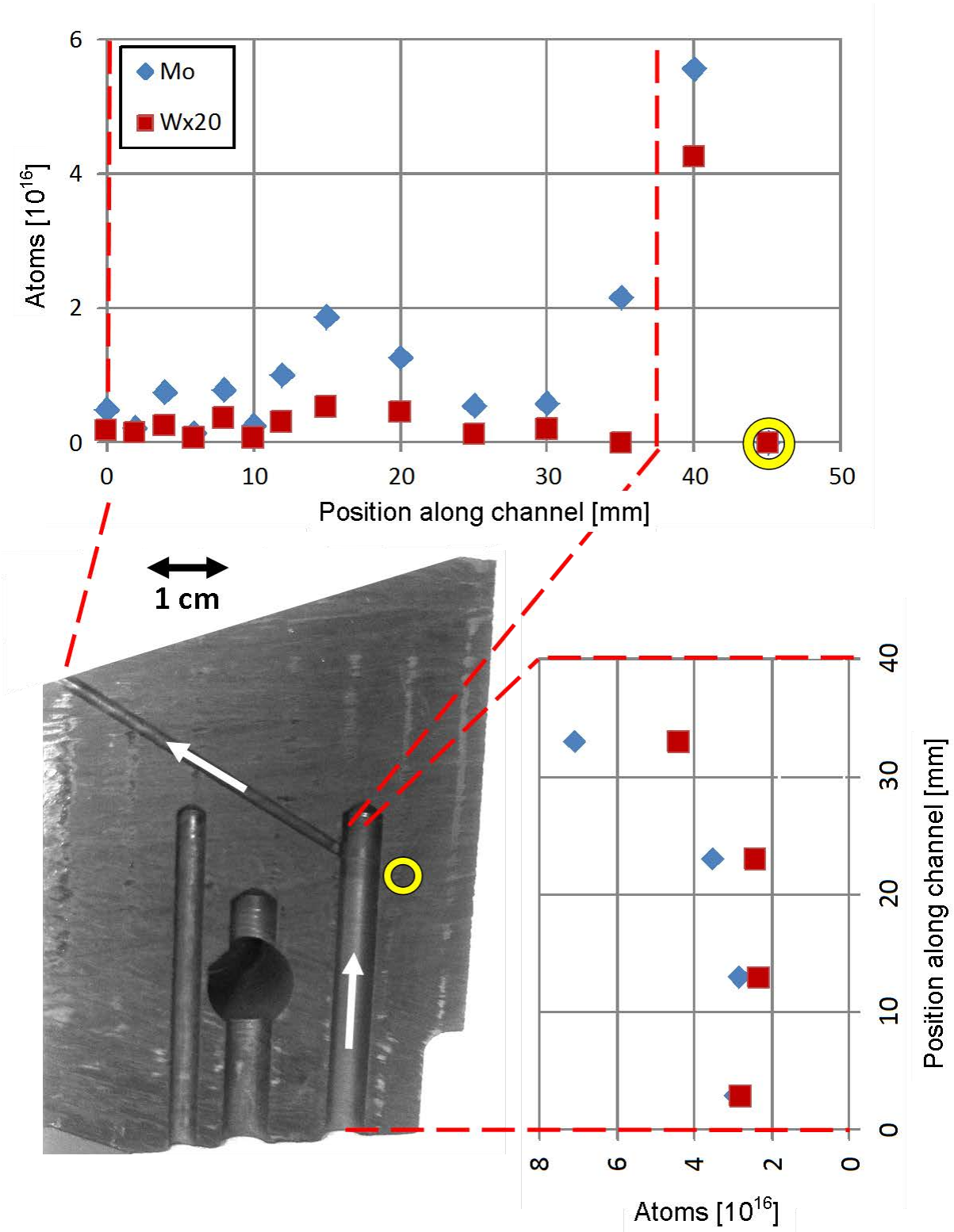

Fig. 9: RBS measurements inside the channels of the graphite block, signals from Mo (blue diamonds) and W (multiplied by 20, red squares). The encircled measurement point was performed on substrate. Injection gas flow is indicated by white arrows.